Astron. Astrophys. 354, 703–713 (2000)

ASTRONOMY AND ASTROPHYSICS

Slow and fast magnetic reconnection

II. High-temperature turbulent-current sheet

B.V. Somov and A.V. Oreshina

Solar Physics Department, Astronomical Institute, Moscow State University, Universitetskii Prospekt 13, Moscow 119899, Russian Federation (somov@sai.msu.su)

Received 27 July 1999 / Accepted 20 October 1999

Abstract. We present a new magnetohydrodynamic model of high-temperature ($T \sim 10^8$ K) turbulent-current sheet forming in regions of magnetic reconnection in the solar corona. A structure of the sheet is studied with allowance for such effects as anomalous resistivity of plasma, radiative cooling, anomalous heat conduction. The relative roles of the two latter factors in the current sheet energy balance are shown. The model describes both the slow regime of reconnection (with O-type magnetic configuration in the center of the sheet) and the fast one (with X-type configuration). Energy release power in the current sheet at the fast regime of reconnection is sufficient to account for solar flares and coronal transients.

Key words: Magnetohydrodynamics (MHD) – Sun: corona – Sun: flares – Sun: magnetic fields

1. Introduction

Magnetic reconnection plays a key role in dynamics of astrophysical plasmas. It serves as a highly efficient engine to convert magnetic energy into thermal and kinetic energies of plasma flows and accelerated particles (e.g., Somov 1994). However, before the *Yohkoh* satellite (e.g., Watanabe et al. 1998), there was no direct clear evidence that it is reconnection that is responsible for the primary release of flare energy. Solar hard and soft X-ray observations on board *Yohkoh* suggest that reconnection indeed takes place in many non-steady phenomena in the corona and in particular, in flares. Reconnection seems to be common to impulsive (compact) and gradual (large-scale) flares. However, in the interpretation of the *Yohkoh* data, 'the basic physics of the reconnection process remains uncertain' (Masuda et al. 1994; Kosugi & Somov 1998).

We investigate a structure of a thin reconnecting current sheet (CS) forming in a super-hot region (Somov 1992) of magnetic reconnection. Our model is characterized by the following features. First, the magnetic field in the CS has a transversal component, i.e. we consider magnetically *non-neutral* CS. Secondly, we study a *longitudinal* structure of the sheet, i.e. a variation of plasma parameters along its width (along the x-axis in Fig. 1). Conditions are described for forming a 'magnetic island' – a region of closed magnetic lines – in the center of the sheet, and also for forming the X-type magnetic configuration.

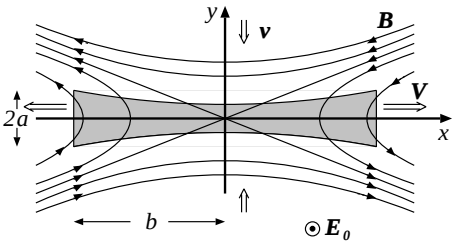

Fig. 1. The model of a thin wide reconnecting current sheet

This investigation is an extension of previous studies performed in the thin-sheet approximation (Somov 1992; Oreshina & Somov 1998 (Paper I in what follows)). In (Somov 1992), estimations of parameters were given which characterize the CS as a whole without allowance for its internal structure. Further the longitudinal (along the width) structure of the sheet was studied in the thin sheet approximation. However, some important factors were not taken into account: radiative cooling, heat conduction, and temperature dependence of resistivity. Oreshina & Somov (1998) took into consideration resistivity calculated in a classical way, that was valid for low temperatures ($T \sim 10^4$ K), for which the computations were made.

The model described below is developed for high temperatures ($T \sim 10^8$ K). It takes into account that the resistivity has an anomalous character under these conditions, in particular, the temperature dependence differs from the classical law. The roles of radiative losses and heat conduction in the energy balance of the sheet are considered.

The necessity of allowing for the anomalous heat conduction and resistivity, instead of the classical ones, was shown, for example, in (Somov 1992). This is due to excitation of waves and wave-particle interaction in turbulent plasma.

The deviation from the classical resistivity was discussed earlier, for example, by Heyvaerts & Priest (1976). They considered a violation of thermal equilibrium in cold ($T \sim 10^4$ K) current sheet and its rapid heating to the temperature of about $10^6 - 10^7$ K. It was noted that during this dynamical process, current-driven microinstabilities may be triggered in the CS,

giving rise to an enhanced resistivity. Turbulent plasma resistivity was estimated according Buneman (1958):

$$\eta = \sigma^{-1}\,; \qquad \sigma = 3.05\,10^{-3}\,n_{\rm e}^{1/2}\,, \quad \mathrm{Mho\ m^{-1}}\,.$$

Here $n_{\rm e}$ is the electron number density. Notice that the CS was studied as a whole without allowance for its internal structure.

An investigation dealing with the anomalous resistivity and heat conduction is performed in some papers by Takakura (1990, 1992), Takakura et al. (1993). They describe a model of an impulsive flare resulting from heat conduction along the loop with an axial electric current. It is assumed that a segment near the top of the coronal loop is heated to above 10^7 K. Due to escaping fast electrons, plasma waves with a high intensity are excited which causes the anomalous resistivity. The initial current starts to decay by an ohmic dissipation under the anomalous resistivity occurring near the loop top and heats this region even more. The enhanced heat conduction spreads in a self-generating way even after the end of the initial minor heating. Takakura calls this process 'the anomalous heat conduction'. The results were obtained by numerical solving the Fokker-Plank equation.

Schumaher & Kleim (1997) discuss 2D compressible MHD simulations of CS dynamics. The anomalous resistivity is given as

$$\eta = c_1\,(|\boldsymbol{j}| - j_{\rm cr}) + c_0\,\eta_0 \qquad \text{for} \quad |\boldsymbol{j}| \geq j_{\rm cr}.$$

Here $j_{\rm cr}$ – the threshold current density, c_1, c_0, η_0 – constants. In the paper by Neukirch et al. (1997) the interaction between magnetic fluxes is investigated by means of 3D MHD simulations. The anomalous resistivity due to current-driven microturbulence is taken into account in the following manner:

$$\eta = \begin{cases} c_2\,(|\boldsymbol{j}| - j_{\rm cr})^2, & \text{if } |\boldsymbol{j}| \geq j_{\rm cr}, \\ 0, & \text{otherwise,} \end{cases}$$

here c_2 is a constant. The model accounts for quasi-stationary soft X-ray emissivity of bright points, flaring of tiny filaments within X-ray bright points, and jet-like flows in the vicinity of bright point features.

Magara & Shibata (1997) deal with plasmoid formation in eruptive flares. They perform a MHD simulation to investigate the evolution of the coronal magnetic field which is initially a force-free one. At some point an initial perturbation is given: region of enhanced resistivity. Here the magnetic reconnection starts and the plasmoid forms. The anomalous resistivity being taken into account is

$$\eta = \begin{cases} \eta_{\rm cr}\left(\left|\dfrac{v_{\rm d}}{v_{\rm cr}}\right| - 1\right), & \text{for } |v_{\rm d}| \equiv \left|\dfrac{j}{\rho}\right| > v_{\rm cr}, \\ 0, & \text{otherwise,} \end{cases}$$

where $v_{\rm d}$ is the relative ion-electron drift velocity, $v_{\rm cr}$ is the threshold velocity, $\eta_{\rm cr}$ is a constant.

So, from this brief review one can conclude that there is no doubt in the anomalous character of the resistivity in the considered conditions, but the dependence of the resistivity on plasma parameters is different according to different authors. In the model described below we try to take into account both the anomalous resistivity and anomalous heat conduction as far as possible most accurately.

A plan of the paper is as follows. In Sect. 2, we formulate a mathematical problem and a solving procedure. Results of numerical computations are presented in Sect. 3. Discussion of results and comparison with previous work are made in Sect. 4.

2. Mathematical description of the problem

2.1. Initial equations

Consider a current sheet sketched in Fig. 1. Magnetic field lines, together with plasma, inflow in it along the y-direction and outflow along the x-direction.

A stationary dissipative 2D MHD problem is investigated. Its aim is to determine a structure of the current sheet: velocity of plasma outflowing, temperature, density, transverse magnetic field in the sheet, and also its thickness as a function of x.

We use the following equations with usual notation:

(1) the continuity equation

$$\mathrm{div}\,\rho\,\boldsymbol{v} = 0\,; \tag{1}$$

(2) the energy conservation

$$-\,\mathrm{div}\,\boldsymbol{G} - \mathcal{L} = 0\,, \tag{2}$$

where

$\boldsymbol{G} = \rho\,\boldsymbol{v}\left(\dfrac{v^2}{2} + w\right) + \boldsymbol{S} + \boldsymbol{F}$ – energy flux density,

$w = \dfrac{5}{2}\,\dfrac{p}{\rho}$ – specific enthalpy,

$\boldsymbol{S} = \dfrac{c}{4\,\pi}\,[\boldsymbol{E} \times \boldsymbol{B}]$ – Poynting's vector,

$\boldsymbol{F}$– density of heat conduction flux,

$\mathcal{L}\,(T,\,n_{\rm e},\,n)$ – radiative loss function;

(3) the equation of momentum conservation

$$\frac{\partial}{\partial\,r_\beta}\,\Pi^*_{\alpha\,\beta} = 0 \quad \text{that is} \quad \begin{cases} \dfrac{\partial}{\partial\,x}\,\Pi^*_{x\,x} + \dfrac{\partial}{\partial\,y}\,\Pi^*_{x\,y} = 0\,, \\ \dfrac{\partial}{\partial\,x}\,\Pi^*_{y\,x} + \dfrac{\partial}{\partial\,y}\,\Pi^*_{y\,y} = 0\,, \end{cases} \tag{3}$$

where the tensor of momentum flux density is

$$\Pi^*_{\alpha\,\beta} = p\,\delta_{\alpha\,\beta} + \rho\,v_\alpha\,v_\beta + \frac{1}{4\,\pi}\left(\frac{B^2}{2}\,\delta_{\alpha\,\beta} - B_\alpha\,B_\beta\right);$$

(4) Ohm's law

$$\boldsymbol{j} = \eta^{-1}\,(\boldsymbol{E} + \frac{1}{c}\,[\boldsymbol{v} \times \boldsymbol{B}])\,; \tag{4}$$

(5) Maxwell's equations

$$\mathrm{rot}\,\boldsymbol{B} = \frac{4\,\pi}{c}\,\boldsymbol{j}\,, \tag{5}$$

$$\mathrm{div}\,\boldsymbol{B} = 0\,. \tag{6}$$

2.2. Transformed equations

We assume that the thickness $2a$ of the CS (Fig. 1) depends only on the coordinate x and remains much smaller than its width $2b$. This approach allows us to consider the CS as a whole along the y-direction. By integrating Eqs. (1)–(4) over the thickness of the sheet (over the variable y) we obtain the one-dimensional problem, i.e. all unknown functions, describing the CS, depend on the coordinate x only.

We assume also that the component $B_{y\,\mathrm{out}}$ of magnetic field near the CS and $B_{x\,\mathrm{in}}$, $B_{y\,\mathrm{in}}$ inside the sheet are small values in comparison with the component $B_{x\,\mathrm{out}}$ outside the sheet, that is the CS differs slightly from the neutral one. Moreover we shall assume that the velocity v of plasma inflowing into the sheet is much smaller than the velocity V of plasma outflowing. Hence we can neglect the terms $\sim v^2$, $B^2_{x\,\mathrm{in}}$ and so on in the equations. This procedure is described more thoroughly in our Paper I.

We shall consider the first quadrant of the coordinate plane, assuming the reconnection process to be symmetrical. A set of equations resulting from the integration is

$$\frac{\mathrm{d}}{\mathrm{d}\,x}\,(\rho\,V a) = -\rho_0\,v, \tag{7}$$

$$\frac{\mathrm{d}}{\mathrm{d}\,x}\,\left[V a\left(\rho\,\frac{V^2}{2}+\frac{5}{2}\,p\right)+a\,F_{x\,\mathrm{in}}(x)\right] = -v\,\left(\frac{5}{2}\,p_0+\frac{B_x^2}{4\pi}\right)-\mathcal{L}\,(T,\,n_\mathrm{e},\,n)\,a - \Big(F_{y\,\mathrm{out}}(x,a)-F_{x\,\mathrm{out}}(x,a)\,a'(x)\Big), \tag{8}$$

$$\frac{\mathrm{d}}{\mathrm{d}\,x}\,\left(\rho\,V^2\,a\right) = -a\,\frac{\mathrm{d}\,p}{\mathrm{d}\,x}+\frac{B_x B_y}{4\pi}\,, \tag{9}$$

$$p = p_0+\frac{B_x^2}{8\pi}\,, \tag{10}$$

$$-\frac{cB_x}{4\pi\,a} = \eta^{-1}\,\left(E_0+\frac{1}{c}\,V\,B_y\right). \tag{11}$$

Here (7) is the continuity Eq., (8) – the energy conservation; (9) and (10) – the equations of momentum conservation along the x- and the y-axis, respectively. Eq. (9) shows that the MHD acceleration inside the CS along the x-axis is simultaneously due to the gas pressure gradient and to the magnetic field line tension. (11) – Ohm's law.

The five Eqs. (7)–(11) contain the following five unknown functions: $a(x)$ – half-thickness of the CS, $V(x)$ – velocity of plasma outflowing from the CS, $\rho(x)$ – density of plasma inside the CS, $T(x)$ – its temperature, $B_y(x) \equiv B_{y\,\mathrm{in}}$ – transverse component of magnetic field inside the CS.

The following functions are postulated to be known. $B_x(x) \equiv B_{x\,\mathrm{out}}$ – the x-component of magnetic field on the inflow sides of the CS – equals that in the vicinity of a thin neutral CS by Syrovatskii (1971):

$$B_x(x) = -h_0\sqrt{b^2-x^2}\,. \tag{12}$$

Here h_0 is a gradient of the external field near a hyperbolic neutral 'point' – the line along the z axis. Velocity $v(x)$ of plasma inflowing into the CS is the y-component of the plasma drift velocity to the CS:

$$\boldsymbol{v}(x) = c\,\frac{[\boldsymbol{E}_0\times\boldsymbol{B}]}{B^2} \approx c\,\frac{E_0}{B_x}\,\boldsymbol{e}_y\,. \tag{13}$$

Here c is the light speed, $\boldsymbol{E}_0 = E_0\,\boldsymbol{e}_z$ is the external electric field.

In Eq. (8) the radiative loss function

$$\mathcal{L}\,(T,\,n_\mathrm{e},\,n) = n_\mathrm{e} n\,L(T), \tag{14}$$

where n_e is the electron number density; $n = n_\mathrm{H}+n_\mathrm{p}$ – the total number density, consisting of the number density of neutral atoms and ions of hydrogen (e.g., Shmeleva & Syrovatskii 1973); $L(T)$ is the 'normalized' radiative loss function (Cox & Tucker 1969; Raymond et al. 1976; Mewe et al. 1986).

Since the temperature of the CS is high ($T \sim 10^8$ K), the heat flux has an anomalous character, instead of the classical one $-\kappa\,\nabla T$, (Manheimer & Klein 1975; Manheimer 1977; Somov 1992):

$$|\boldsymbol{F}| = F_\mathrm{an} = \frac{n_\mathrm{e}\,(k_\mathrm{B}\,T_\mathrm{e})^{3/2}}{m_\mathrm{i}^{1/2}}\;f(\theta)\,. \tag{15}$$

Here k_B is the Boltzmann constant, m_i is the ion mass, θ is the ratio of electron and ion temperatures: $\theta = T_\mathrm{e}/T_\mathrm{i}$. For $T_\mathrm{e}/T_\mathrm{i} \gg 1$ $f(\theta) \approx 1$. Heat flux is assumed to propogate only along the field lines. In order to simplify the energy equation, suppose that the x-component of magnetic field inside the sheet is vanishing. Then heat flux inside the sheet $F_{x\,\mathrm{in}} = 0$. On the surface of the sheet we have

$$F_{x\,\mathrm{out}}(x,a) = F_\mathrm{an}\,\cos\xi\,, \tag{16}$$

$$F_{y\,\mathrm{out}}(x,a) = F_\mathrm{an}\,\sin\xi\,. \tag{17}$$

Here ξ is the angle between field lines and the x-axis near the sheet,

$$|\mathrm{tg}\,\xi| = \left|\frac{B_{y\,\mathrm{out}}}{B_{x\,\mathrm{out}}}\right|\,. \tag{18}$$

The component $B_{y\,\mathrm{out}}$ is determined from the continuity equation for the normal component of the field on the sheet surface:

$$B_{\mathrm{n\,out}} - B_{\mathrm{n\,in}} = 0\,. \tag{19}$$

Hence

$$B_{y\,\mathrm{out}} = B_{x\,\mathrm{out}}\,\frac{\mathrm{d}\,a}{\mathrm{d}\,x}+B_{y\,\mathrm{in}}\,. \tag{20}$$

The dependence of the resistivity on the temperature in the high-temperature turbulent-current sheet also differs from the classical one

$$\eta_\mathrm{cl} = \sigma_\mathrm{cl}^{-1}, \qquad \sigma_\mathrm{cl} = C_0\,T^{3/2}, \tag{21}$$

where $C_0 = 1.4\,10^8/\ln\Lambda$, $\ln\Lambda$ is the Coulomb logarithm. According to de Kluiver et al. (1991), the anomalous resistivity due to current instabilities can be described by the following expression

$$\frac{\eta_{\rm cl}}{\eta} \approx 0.1\,\frac{E_{\rm cr}}{E}\,, \tag{22}$$

where $E_{\rm cr}$ is Dreicer's critical field

$$E_{\rm cr} \;=\; 0.55\,10^{-17}\;\frac{n\,({\rm m}^{-3})}{T_{\rm e}\,({\rm eV})}\;\ln\Lambda\,, \qquad {\rm V/m} \;=$$

$$=\; 2.13\,10^{-12}\;\frac{n\,({\rm cm}^{-3})}{T_{\rm e}\,({\rm K})}\;\ln\Lambda\,, \qquad {\rm CGS}. \tag{23}$$

$E_{\rm cr}$ is the electric field strength by which an electron gains a drift velocity equivalent to the electron thermal velocity, $v_{_{T_{\rm e}}}$, within the electron-ion collision time $1/\nu_{\rm ei}$.

Instead of using different complicated models to find anomalous resistivity in different regimes of plasma turbulence (see Somov 1992), we adopt an empirical approach by de Kluiver et al. (1991) and will determine the properties of turbulent CS using the 1D Eqs. (7)–(11) supplemented by the experimentally tested relationship (22).

Taking into account Eqs. (21) and (23), Eq. (22) can be rewritten as follows:

$$\eta = 5.6\,10^{-20}\;\frac{E}{T^{1/2}\,\rho}\,, \qquad {\rm s}\,. \tag{24}$$

Pressure p and temperature T inside the CS are related by the ideal gas state equation:

$$p = n_{\rm e}\,k_{\rm B}\,T = \frac{\rho\,k_{\rm B}\,T}{m_{\rm i}}\,. \tag{25}$$

We assume here that $m_{\rm i} = m_{\rm p}$ and $T = T_{\rm e} \gg T_{\rm i}$ that is reasonable for plasma inside the high-temperature turbulent-current sheet. Outside the sheet $T_{\rm e} = T_{\rm i} = T_0$ and

$$p_0 = 2\,n_0\,k_{\rm B}\,T_0 = \frac{2\,\rho_0\,k_{\rm B}\,T_0}{m_{\rm i}}\,. \tag{26}$$

External plasma parameters: electron number density n_0, temperature T_0, magnetic field gradient h_0, and electric field E_0, and also current sheet half-width b are assumed to be constants.

Boundary conditions for the obtained closed set of Eqs. (7)–(11) ensue from the problem symmetry and are of the form:

$$V(0) = B_y(0) = 0\,, \tag{27}$$

$$\left.\frac{{\rm d}\,T}{{\rm d}\,x}\right|_{x=0} = \left.\frac{{\rm d}\,\rho}{{\rm d}\,x}\right|_{x=0} = \left.\frac{{\rm d}\,a}{{\rm d}\,x}\right|_{x=0} = 0\,. \tag{28}$$

2.3. Dimensionless equations and parameters of the problem

The set of Eqs. (7)–(11) can be rewritten for dimensionless functions. The only independent variable x and all functions are divided by their characteristic values, and the dimensionless variables are marked by an asterisk:

$$x^* = \frac{x}{b}\,; \tag{29}$$

$$V^* = \frac{V}{V_{\rm A}}\,, \quad V_{\rm A} = \frac{B_0}{\sqrt{4\pi\,\rho_0}}\,, \quad B_0 = h_0\,b\,; \tag{30}$$

$$\rho^* = \frac{\rho}{\rho_0}\,, \quad T^* = \frac{T}{T_0}\,; \tag{31}$$

$$B_y^* = \frac{B_y}{\varepsilon\,B_0}\,, \quad \varepsilon = \frac{V_{\rm d}}{V_{\rm A}}\,, \quad V_{\rm d} = c\,\frac{E_0}{B_0}\,; \tag{32}$$

$$p^* = \frac{p}{p_{\rm m}}\,, \quad p_{\rm m} = \frac{B_0^2}{8\pi}\,; \quad L^* = \frac{L}{L_{\rm max}}\,; \tag{33}$$

$$\eta^* = \frac{\eta}{\eta_0} = T^{*-1/2}\,\rho^{*-1}\,, \quad \eta_0 = 5.6\,10^{-20}\,\frac{E_0}{T_0^{1/2}\,\rho_0}\,; \tag{34}$$

$$a^* = \frac{a}{a_0}\,, \quad a_0 = \frac{c^2\,\eta_0}{4\pi\,V_{\rm d}}\,; \tag{35}$$

$$B_x^* = \frac{B_x}{B_0} = -\sqrt{1-x^{*2}}\,; \tag{36}$$

$$v^* = \frac{v}{V_{\rm d}} = -\frac{1}{\sqrt{1-x^{*2}}}. \tag{37}$$

Here a_0 is the characteristic value of the CS half-thickness; B_0, $p_{\rm m}$, $V_{\rm A}$, and $V_{\rm d}$ are the characteristic values of magnetic field, magnetic pressure, Alfvén velocity, and drift velocity outside the CS, respectively; $L_{\rm max} = 10^{-21}\,{\rm erg\,cm^3\,s^{-1}}$ is the maximum value of the radiative loss function $L(T)$,

So, Eqs. (7)–(11) takes the following form:

$$\frac{\rm d}{{\rm d}\,x^*}\,(\rho^*\,V^*\,a^*) = -\frac{1}{\alpha}\,v^*, \tag{38}$$

$$\frac{\rm d}{{\rm d}\,x^*}\left(V^*\,a^*\,(\rho^*\,V^{*2} + \frac{5}{2}\,p^*)\right) =$$

$$= -\frac{1}{\alpha}\,v^*\,\left(\frac{5}{2}\,\beta + 2\,B_x^{*2}\right) - \frac{\alpha_{\rm r}}{\alpha}\,\rho^{*2}\,a^*\,L^* -$$

$$-\frac{1}{4}\,\beta^{3/2}\,\rho^*\,T^{*3/2}\,\left(\frac{1}{\alpha\,\varepsilon}\,\sin\xi - a^{*\prime}\,\cos\xi\right), \tag{39}$$

$$\frac{\rm d}{{\rm d}\,x^*}(\rho^*\,V^{*2}\,a^*) = a^*\,x^* + \frac{1}{\alpha}\,B_x^*\,B_y^*, \tag{40}$$

$$p^* = \beta + 1 - x^{*2}, \tag{41}$$

$$-\frac{B_x^*}{a^*} = \eta^* * -1\,(1 + B_y^*). \tag{42}$$

This set of equations depends on four parameters. The first one, ε, characterizes the rate of reconnection in the CS (in the stationary case, the reconnection rate equals to the characteristic drift velocity $V_{\rm d}$ to the current sheet):

$$\varepsilon = \frac{V_{\rm d}}{V_{\rm A}} = (4\,\pi\,m_{\rm i})^{1/2}\,c\;\left(n_0^{1/2}\,E_0\,h_0^{-2}\,b^{-2}\right)\,. \tag{43}$$

The second parameter, α, can be considered as a description of the sheet dimensions and also of the reconnection rate:

$$\alpha = \frac{a_0}{b}\,\frac{V_{\rm A}}{V_{\rm d}} = \tag{44}$$

$$= (4\pi m_{\rm i})^{-3/2}\,5.6\,10^{-20}\left(n_0^{-3/2}T_0^{-1/2}E_0^{-1}h_0^3b^2\right). \tag{45}$$

The third parameter, β, is the ratio of external gas pressure to magnetic pressure:

$$\beta = \frac{p_0}{p_{\rm m}} = \frac{8\pi\,p_0}{B_0^2} = 16\,\pi\,k_{\rm B}\ \left(n_0\,T_0\,h_0^{-2}\,b^{-2}\right). \tag{46}$$

The last parameter, $\alpha_{\rm r}$, evaluates the role of radiative losses. The larger value of $\alpha_{\rm r}$, the larger role of radiative losses,

$$\alpha_{\rm r} = \frac{L_{\max}}{L_0} = \frac{1.12\,10^{-19}\,L_{\max}}{m_{\rm i}}\ \left(n_0\,T_0^{-1/2}\,E_0^{-1}\right);$$

$$L_0 = \frac{E_0^2\,m_{\rm i}^2}{2\,\rho_0^2\,\eta_0}, \quad {\rm erg\,cm^3\,s^{-1}}. \tag{47}$$

3. Numerical computations

3.1. Selection of parameters

The computations have been performed for four sets of the dimensionless parameters indicated in Table 1.

Parameters $\alpha, \beta, \varepsilon, \alpha_{\rm r}$ are determined by the external parameters: n_0, T_0, E_0, and h_0, and also by half-width of the sheet b (see Eqs. (43)–(47)). So, values from Table 1 may correspond, for instance, to plasma parameters given in Table 2. Transition from set I to set III corresponds to enhancement of electric field E_0. Set IV differs from set III in increasing the width of the sheet.

In Table 3 additional plasma characteristics are given, which are calculated using the data from Table 2. They are also the coefficients of transition from the dimensionless values to the dimensional ones (see Eqs. (29)–(37)). As we can see, in variants I–III, the drift velocity to the sheet gradually increases. It means that the reconnection rate increases also. So we shall see below the change of the structure of the CS in dependence on the reconnection rate.

3.2. Description of results

Results of numerical computations are shown in Figs. 2–4. They demonstrate variations along the sheet width (i.e. along the coordinate $x^* = x/b$) of the velocity of plasma outflowing from the sheet $V^* = V/V_{\rm A}$ and the plasma density inside the sheet $\rho^* = \rho/\rho_0$ (Fig. 2), plasma temperature $T(x^*)$ and half-thickness of the sheet $a^* = a/a_0$ (Fig. 3), and also the transverse component of the field $B_y^* = B_y/\varepsilon\,B_0$ (Fig. 4). Point $x^* = 0$ corresponds to the center of the CS. Numbers near the curves indicate the set of parameters $\{\alpha, \beta, \varepsilon, \alpha_{\rm r}\}$, according to Table 1, for which the solutions are obtained.

Note that computations have been performed up to the point $x^* = 0.98$. It is related to the fact that at $x^* = 1.0$ the velocity of plasma inflowing in the sheet $v^* = -1/\sqrt{1-x^{*2}}$ equals infinity. Therefore the approximation used is not valid in the vicinity of the point $x^* = 1.0$.

Solutions obtained without taking into account radiative losses and heat conduction are shown by dashed curves. Solutions that take into account these factors are shown by solid curves. It is worth noting however that the role of radiative losses is small ($\alpha_{\rm r} \sim 10^{-4} - 10^{-2}$), so the difference between the solid and dashed curves is mainly due to heat conduction only (see also Sect. 3.3).

Fig. 4 demonstrates that the transverse component of magnetic field strongly depends on the reconnection rate. For a small reconnection rate (curve I) B_y^* changes the sign from positive to negative at some point x^*, that is a 'magnetic island' – region of closed field lines – appears in the center part of the CS (Fig. 5a). For a higher reconnection rate (curve II–IV) B_y^* has a negative sign, which corresponds to X-type magnetic configuration (Fig. 5b). So, depending on the reconnection rate, two regimes of reconnection are possible: the slow one, with magnetic configuration of O-type, or magnetic island, and the fast one, with X-type magnetic configuration.

In the O-type configuration magnetic field lines are closed and hence heat conduction as a mechanism of energy output from the sheet does not play any role. This is why the dashed and solid curves in variant I coincide.

As Figs. 2–4 show, the allowance for heat conduction makes the current sheet colder, denser and thinner, with slower velocity of plasma outflowing.

Table 1. Parameters of the problem

Set	α	β	ε	$\alpha_{\rm r}$
I	37	$1.1\,10^{-2}$	$1.1\,10^{-7}$	$1.3\,10^{-2}$
II	3.7	$1.1\,10^{-2}$	$1.1\,10^{-6}$	$1.3\,10^{-3}$
III	0.37	$1.1\,10^{-2}$	$1.1\,10^{-5}$	$1.3\,10^{-4}$
IV	3.7	$1.1\,10^{-3}$	$1.1\,10^{-6}$	$1.3\,10^{-4}$

Table 2. External parameters and half-width of the sheet

Set	n_0, ${\rm cm^{-3}}$	T_0, K	E_0, CGS	h_0, ${\rm Gs\,cm^{-1}}$	b, cm
I	10^{10}	10^6	$5\,10^{-8}$	$5\,10^{-7}$	$1.6\,10^8$
II	10^{10}	10^6	$5\,10^{-7}$	$5\,10^{-7}$	$1.6\,10^8$
III	10^{10}	10^6	$5\,10^{-6}$	$5\,10^{-7}$	$1.6\,10^8$
IV	10^{10}	10^6	$5\,10^{-6}$	$5\,10^{-7}$	$5.0\,10^8$

Table 3. Coefficients of transition from the dimensionless values to the dimensional ones

Set	ρ_0, ${\rm g\,cm^{-3}}$	B_0, Gs	$V_{\rm d}$, ${\rm cm\,s^{-1}}$	$V_{\rm A}$, ${\rm cm\,s^{-1}}$	a_0, cm
I	$1.7\,10^{-14}$	80	$1.9\,10^1$	$1.7\,10^8$	$6.4\,10^2$
II	$1.7\,10^{-14}$	80	$1.9\,10^2$	$1.7\,10^8$	$6.4\,10^2$
III	$1.7\,10^{-14}$	80	$1.9\,10^3$	$1.7\,10^8$	$6.4\,10^2$
IV	$1.7\,10^{-14}$	250	$5.9\,10^2$	$5.5\,10^8$	$2.0\,10^3$

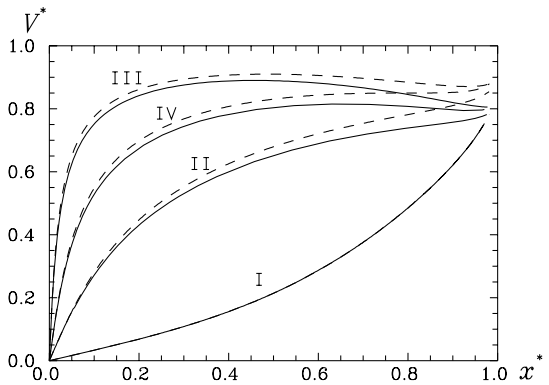

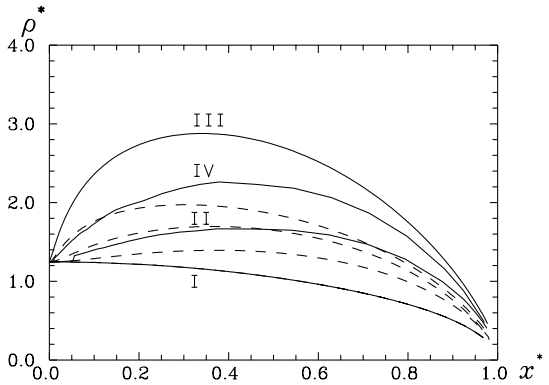

Fig. 2. Velocity of plasma outflowing from the current sheet and plasma density obtained for the case when radiative losses and heat conduction are not taken into account (dashed lines) and results taking into account these effects (solid lines). Numbers near the curves indicate the set of parameters for which the computations have been performed

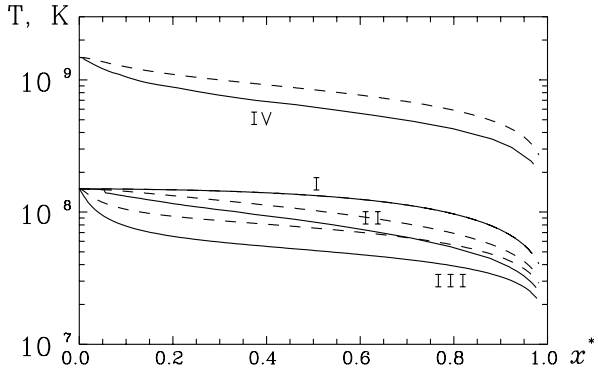

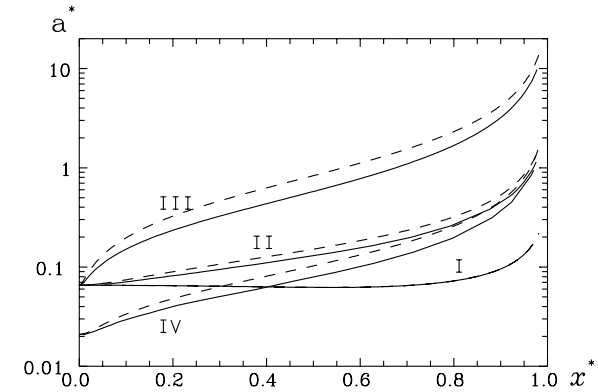

Fig. 3. Plasma temperature and thickness of the sheet obtained for the case when radiative losses and heat conduction are not taken into account (dashed lines) and results taking into account these effects (solid lines). Numbers near the curves indicate the set of parameters for which the computations have been performed

Comparing variants I–III which are charecterized by increasing electric field E_0 and hence by increasing reconnection rate, we see that it leads first of all to the change of magnetic configuration as was mentioned above, and also to the acceleration of plasma outflowing from the sheet, to its compression and cooling.

Consider now the structure of the CS with larger, than in variant III, width (variant IV). In this case the magnetic field near the sheet has increased also: $B_0 = h_0\, b$ (see Table 3). Correspondingly, plasma drift velocity to the sheet has slowed down and characteristic velocity of plasma outflowing has accelerated. Characteristic time of plasma staying in the sheet $\tau = b/V_{\rm A}$ has remained the same: $\tau = 1.6\,10^8\ {\rm cm}/1.7\,10^8\ {\rm cm\,s^{-1}} = 0.9\ {\rm s}$ in variant III, $\tau = 5.0\,10^8\ {\rm cm}/5.5\,10^8\ {\rm cm\,s^{-1}} = 0.9\ {\rm s}$ in variant IV.

Looking at Figs. 2–4, dimensionless velocity of outflowing V^* has slowed down. However dimensional velocity $V = V_{\rm A}\, V^*$ has accelerated. Plasma density in the sheet has decreased somewhat and the temperature has increased by an order of magnitude. Component B_y^* of magnetic field has not undergone large changes, but the ratio $B_{y\,{\rm in}}/B_{x\,{\rm out}} = \varepsilon\, B_y^*/B_x^*$ has decreased. Dimensional thickness of the sheet $a = a_0\, a^*$ has remained practically unchanged: $a(0) = 6.4\,10^2({\rm cm})\ 6.5\,10^{-2} = 42\ {\rm cm}$ in variant III, and $a(0) = 2.0\,10^3({\rm cm})\ 2.1\,10^{-2} = 42\ {\rm cm}$ in variant IV.

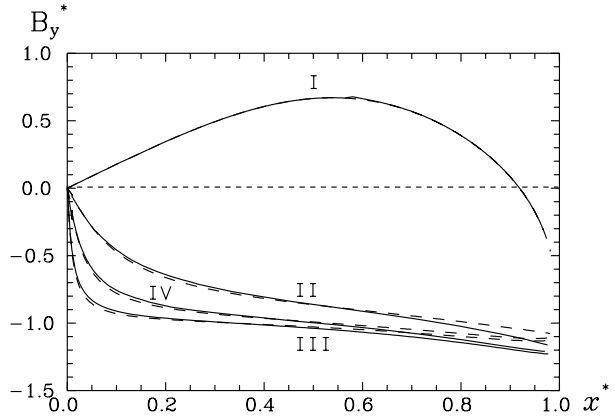

Fig. 4. Transverse magnetic field in the sheet obtained for the case when radiative losses and heat conduction are not taken into account (dashed lines) and results taking into account these effects (solid lines). Numbers near the curves indicate the set of parameters for which the computations have been performed

Thus it can be concluded that in the larger sheet, approximately for the same time as in the small sheet, plasma is acceler-

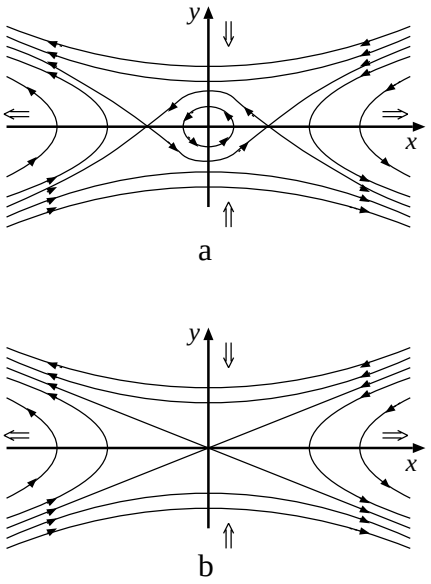

Fig. 5a and b. Configurations of magnetic field in the reconnecting current sheet: **a** O-type ('magnetic island') – slow regime of reconnection; **b** X-type – fast regime of reconnection

ated to faster velocities and is heated up to higher temperatures, that is the efficiency of reconnection is increased.

3.3. Energy balance of the current sheet

The aim of this subsection is to clear up the roles which various factors play in the energy balance of the CS. For this, turn to energy Eq. (39):

$$\frac{\mathrm{d}}{\mathrm{d}\,x^*}\left(V^*\,a^*\,(\rho^*\,V^{*2}+\frac{5}{2}\,p^*)\right)=$$

$$=-\frac{1}{\alpha}\,v^*\,\left(\frac{5}{2}\,\beta+2\,B_x^{*2}\right)-\frac{\alpha_{\rm r}}{\alpha}\,\rho^{*2}\,a^*\,L^*-$$

$$-\frac{1}{4}\,\beta^{3/2}\,\rho^*\,T^{*3/2}\,\left(\frac{1}{\alpha\,\varepsilon}\,\sin\xi-a^{*\prime}\,\cos\xi\right).$$

Its left part, which can be rewritten also in the following manner

$$\frac{\mathrm{d}}{\mathrm{d}\,x}\int\limits_{-a(x)}^{a(x)}G_x(x,\,y)\,\mathrm{d}y, \qquad (48)$$

describes variation (along the sheet width) of the energy flux, consisting of kinetic energy of plasma and specific enthalpy (see Eq. (2)). The first term of the right part, SI, constitutes the energy which is input in the sheet. It consists of internal energy of plasma and magnetic field energy. As $\beta \ll 1$ in considered cases, the main role belongs to the latter. Note that $\mathrm{SI} > 0$ since $v^* = -1/\sqrt{1-x^{*2}} < 0$. The second term, SL, describes the radiative losses. The role of this term in the common energy balance is not large: $\mathrm{SL} \sim 10^{-7}$ in variant I, 10^{-6} in variant II, 10^{-5} in variant III, and 10^{-6} in variant IV. The third term,

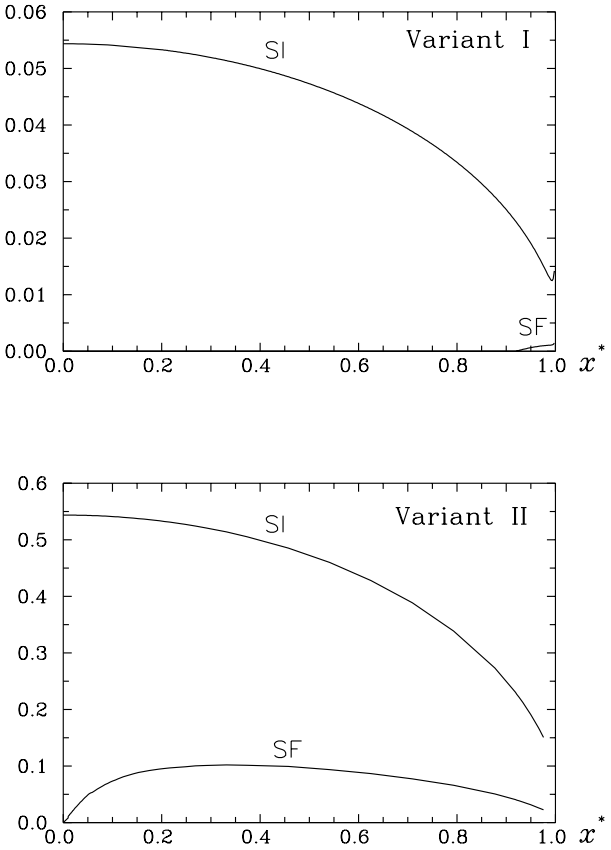

Fig. 6. Terms of energy equation in variants I and II: SI – energy which is input into the sheet, SF – energy losses due to heat conduction

SF, is the energy losses due to heat conduction. The absolute values of the terms SI and SF in dependence on x^* are shown in Figs. 6 and 7. There is no energy loss due to heat conduction in variant I because of magnetic island with closed field lines. In this case magnetic field energy converts into the thermal and kinetic energy of outflowing plasma. In cases II–IV some part of it is lost by the sheet due to heat conduction.

The relative role of heat conduction in the cases of X-configuration (variants II–IV) does not change: $\mathrm{SF/SI} \approx \mathrm{const} \approx 0.2$. This situation is connected with the fact that both processes (energy input into the sheet and energy output due to heat conduction) are controlled by one and the same parameter – the rate of reconnection. The larger reconnection rate, the larger the energy inputs into the sheet, i.e. the larger term SI. On the other hand, the angle between magnetic field lines and sheet surface also increases leading to enhancing heat conduction, i.e. term SF.

Numerical estimations show that the role of radiation is small in the high-temperature turbulent-current sheet. However the allowance for radiative losses in the energy equation yields qualitatively new results: existence of low-temperature current sheets also becomes possible. From a mathematical point of view, this is connected with the character of function $L(T)$ which has a maximum at the temperature of $T_1 \approx 2.6\,10^5$ K and a minimum at $T_2 \approx 1.7\,10^7$ K. As a result, one value

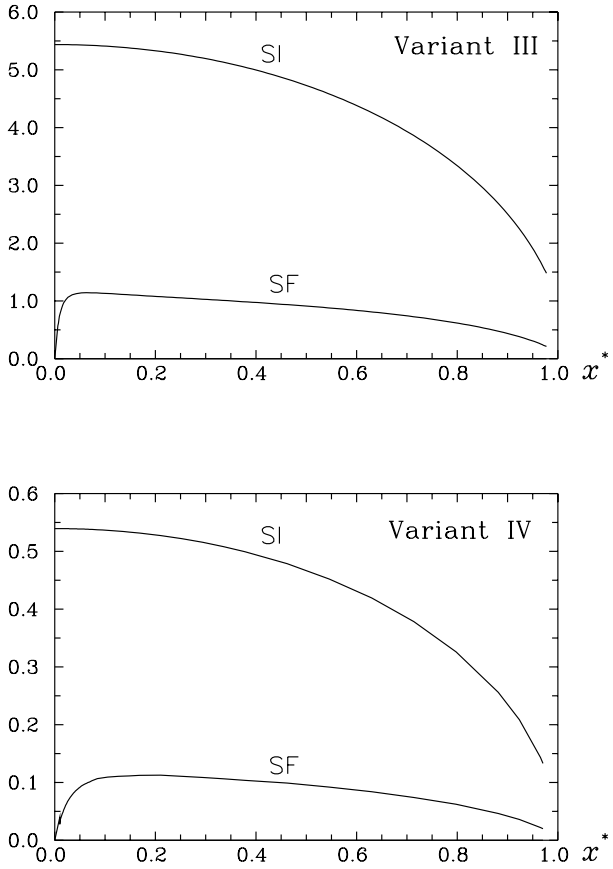

Fig. 7. Terms of energy equation in variants III and IV: SI – energy which is input into the sheet, SF – energy losses due to heat conduction

$L(T)$ can correspond to three values of T. So three solutions of energy equation are possible. The intermediate solution, connected with the region $[T_1,\, T_2]$, is unstable. Here radiative losses decrease with increasing temperature. Therefore some enhancement of temperature relative to its equilibrium value results in a decrease of radiative losses and hence in further plasma heating, and vice versa: some temperature decrease leads to further cooling. The low-temperature and high-temperature solutions are stable. The low-temperature solution with $T \sim 10^4$ K exists in our computations but we do not show it because this is beyond the framework of the paper (for instance in this case the classical resistivity must be taken into account instead of the anomalous one, and so on).

4. Discussion and conclusion

In this section we compare the new results presented above with those of previous studies. First of all, the new model is compared with a test one — the two-temperature model of high-temperature turbulent-current sheet (HTCS), described in (Somov 1992). It is called the two-temperature model because it takes into account a difference between electron and ion temperatures that influences the anomalous resistivity value and also the threshold of plasma turbulence excitation.

Initial equations constitute the order of magnitude relations for the CS as a whole without allowance for its structure:

$$n_0\, V_{\rm d}\, b = n\, V\, \xi\, b\,, \tag{49}$$

$$\frac{B_0^2}{8\,\pi} = n\, k_{\rm B}\, T(1+\theta^{-1})\,, \tag{50}$$

$$n\, k_{\rm B}\, T(1+\theta^{-1}) = \frac{1}{2}\, m_{\rm i}\, n\, V^2\,, \tag{51}$$

$$\frac{c\, B_0}{4\,\pi\, a} = \frac{E_0}{\eta_{\rm ef}}\,, \tag{52}$$

$$\chi_{\rm ef}\, \frac{B_0^2}{4\,\pi}\, V_{\rm d}\, b = \frac{5}{2}\, n\, k_{\rm B}\, T\, V\, \xi\, b + f(\theta)\, \frac{n\,(k_{\rm B}\, T)^{3/2}}{m_{\rm i}^{1/2}}\, \xi b\,, \tag{53}$$

$$(1-\chi_{\rm ef})\, \frac{B_0^2}{4\,\pi}\, V_{\rm d}\, b = \left(\frac{1}{2}\, m_{\rm i}\, n\, V^2 + \frac{5}{2\theta}\, n\, k_{\rm B} T\right) V \xi b\,. \tag{54}$$

Here (49) is the continuity Eq., (50) and (51) are the equation of momentum conservation along the y- and the x-axis, respectively, (52) – Ohm's law, (53) and (54) are the energy equations for electron and ion components. The designations are the same as those adopted earlier; $\xi = B_y/B_x$ is the relative value of the transversal component of magnetic field in the sheet, $\theta = T_{\rm e}/T_{\rm i}$ is the relation of electron and ion temperatures, $T \equiv T_{\rm e}$, $\eta_{\rm ef}$ is the effective resistivity, $\chi_{\rm ef}$ is the relative part of electron Joule heating.

Eqs. (49), (53) and (54) suppose that plasma outflows from the sheet along the field lines under the influence of gas pressure gradient. The effective scale of plasma outflowing from the sheet and heat conduction cooling is proportional to the value ξb in this case.

A study is made of the turbulence due to ion-cyclotron and ion-acoustic instabilities. Four regimes of the turbulence are possible: threshold regime of the ion-cyclotron turbulence (ICT), saturated regime of the ICT, threshold regime of the ion-acoustic turbulence (IAT), and saturated regime of the IAT. For each regime the conditions of existence (the intervals of possible values ξ and T) and corresponding values $\eta_{\rm ef}$ and $\chi_{\rm ef}$ are determined.

For the threshold regimes of the ICT and IAT the characteristics of the current sheet are obtained for fixed values of the external parameters n_0, h_0, and E_0, and also for the dimensionless parameter ξ. Magnetic reconnection rate $V_{\rm d}$ and energy release power P at the threshold regime of IAT are found to be some orders of magitude larger than at the threshold regime of ICT. Limitation of the reconnection rate is attributed to the fact that the resistivity $\eta_{\rm ef}$ is not large at the ICT. The same conclusion is valid for the saturated regime of ICT also. At the threshold regime of IAT, the energy release power and reconnection rate are sufficient to account for solar flares and slow coronal transients. At the saturated regime of IAT, larger values of these parameters may be obtained, sufficient for the interpretation of fast coronal transients.

An example of the high-temperature turbulent-current sheet computation at the threshold regime of IAT is given in the left column of Table 4.

Table 4. Parameters of HTCS obtained in the test and new models

Test	New model
Threshold regime of IAT.	
$\theta \approx 6.5, \quad n/n_0 \approx 4.8$	$\theta = \infty$
Given parameters	
$n_0 = 10^{10}\ \mathrm{cm}^{-3}$	$n_0 = 10^{10}\ \mathrm{cm}^{-3}$
$E_0 = 10^{-3}$ CGS	$E_0 = 10^{-3}$ CGS
$h_0 = 5\,10^{-7}\ \mathrm{Gs\,cm}^{-1}$	$h_0 = 5\,10^{-7}\ \mathrm{Gs\,cm}^{-1}$
$\xi = 10^{-3}$	$b = 1.6\,10^{8}$ cm
	$T_0 = 10^{6}$ K
Computed parameters	
$a = 22$ cm	$a \sim 42$ cm $- 6\,10^{5}$ cm
$b = 1.6\,10^{8}$ cm	$\xi \approx 2\,10^{-3}$
$T = 2.1\,10^{7}$ K	$T \approx 7\,10^{7}$ K
$\eta = 1.2\,10^{-13}$ s	$\eta \approx 1.9\,10^{-13}$ s
$B_0 = 80$ Gs	$B_0 = 80$ Gs
$V_\mathrm{d} = 3.7\,10^{5}\ \mathrm{cm\,s}^{-1}$	$V_\mathrm{d} = 3.7\,10^{5}\ \mathrm{cm\,s}^{-1}$
$P/l = 10^{17}\ \mathrm{erg\,cm}^{-1}\,\mathrm{s}^{-1}$	$P/l = 1.2\,10^{17}\ \mathrm{erg\,cm}^{-1}\,\mathrm{s}^{-1}$
	$n \approx 2\,10^{10}\ \mathrm{cm}^{-3}$

Table 5. Dimensionless parameters and coefficients of transition from dimensionless values to dimensional ones in the new model

Dimensionless parameters	Coefficients of transition from dimensionless values to dimensional ones
$\alpha = 1.9\,10^{-3}$	$V_\mathrm{A} = 1.7\,10^{8}\ \mathrm{cm\,s}^{-1}$
$\beta = 0.01$	$\rho_0 = 1.7\,10^{-14}\ \mathrm{g\,cm}^{-3}$
$\varepsilon = 2.1\,10^{-3}$	$B_0 = 80$ Gs
$\alpha_\mathrm{r} = 6.7\,10^{-7}$	$a_0 = 6.4\,10^{2}$ cm

The new model of the CS somewhat differs from the test one. First of all, initially a 2D problem is formulated and then it is reduced to quasi-one-dimensional problem by integrating over the thickness of the sheet. As a result, Eqs. (7)–(11) differ from (49)–(54) in dependence on x; moreover plasma outflows from the sheet across its sides, not along field lines (compare Eqs. (7) and (49)). Secondly, the new problem assumes $T_\mathrm{e} \gg T_\mathrm{i}$ that corresponds $\theta = \infty$, $\chi_\mathrm{ef} = 1$, $f(\theta) = 1$ (instead of $\theta = 6.5$, $\chi_\mathrm{ef} = 0.85$, $f(\theta) = 10.7$ in the test problem). Thirdly, the value ξ is computed and b is given in the new model in contrast to the test.

To compare these two models, Eqs. (38)–(42) of the new model have been solved for the same values n_0, h_0, E_0 and b as in the test problem. Results are shown in Fig. 8 and in Table 4 in the right column. Corresponding dimensionless parameters and coefficients of transition from dimensionless values to dimensional ones in the new model are given in Tabel 5.

Comparing the results obtained in the framework of the new and the test models, one can conclude the following.

1. The current sheet in the new model is somewhat more rarefied ($n/n_0 \approx 2$ instead of 4.8) and hotter ($T \approx 7\,10^{7}$ K instead of $2.1\,10^{7}$ K); relative value of transversal field $B_y/B_x = \varepsilon\, B_y^*/B_x^* \approx 2\,10^{-3}$ (instead of 10^{-3}). That is all these values have not undergone large changes.

2. The thickness of the sheet has become significantly larger. Only at the center, at $x = 0$, it coincides with the estimation of the test model by the order of magnitude: $a(0) = a_0\, a^*(0) = 6.4\,10^{2}\,(\mathrm{cm}) \times 6.5\,10^{-2} = 42$ cm (instead of 22 cm). On average $a^*(x^*) \sim 10^{3}$, i.e. $a(x) \sim 6\,10^{5}$ cm. This large thickness is due to necessity of outflowing large amounts of plasma, that inflows into the sheet at this very fast reconnection (see Eq. (7)). In the test problem plasma outflows from the sheet along field lines, which is not connected with the sheet thickness (Eq. (49)). The latter is defined as a region of anomalous resistivity, responsible for reconnection (see Ohm's law (52)).

Note that in spite of large thickness, the current sheet remains turbulent in the new model. Indeed, the state of current-driven turbulence can be provoked by applying a sufficiently large electric field enchancing E_cr (see Eq. (23)). For $T = 7\,10^{7}$ K and $n = 2\,10^{10}\ \mathrm{cm}^{-3}$ one obtains $E_\mathrm{cr} = 1.4\,10^{-8}$ CGS, that is less than $E_0 = 10^{-3}$ CGS adopted in our model. Resistivity in this case can be estimated using Eq. (22), that gives $\eta = 1.9\,10^{-13}$ s.

However the question about the type of turbulence – ion-acoustic or ion-cyclotron – in the new model remains open for the present.

3. Energy balance of the CS has insignificantly changed. To show this, one can estimate the energy coming in the sheet per $1\ \mathrm{cm}^2$ of the surface per 1 s (see Eq. (8)):

$$\mathrm{SI} = V_\mathrm{d}\left(\frac{5}{2}\,p_0 + \frac{B_0^2}{4\,\pi}\right) \approx 1.9\,10^{8} \quad \mathrm{erg\,cm}^{-2}\,\mathrm{s}^{-1}\,.$$

Hence the total energy released per unit of the sheet length per unit of the time is

$$P/l = 4\ \mathrm{SI}\ b = 1.2\,10^{17} \quad \mathrm{erg\,sm}^{-1}\,\mathrm{s}^{-1}\,.$$

So, the obtained value P/l is in good agreement with the result of the test model (see Table 4). For sheet length $l \sim 10^{10}$ cm we have $P \sim 10^{27}\ \mathrm{erg\,s}^{-1}$, which is comparable with energy release power in solar flares and coronal transients.

The relative role of heat conduction in the new model is somewhat less than in the test. As Fig. 8 shows, $\mathrm{SF/SI} \approx 0.2$. The corresponding value in the test model can be estimated using energy equation for electron component (53):

$$\mathrm{SI} = \chi_\mathrm{ef}\,\frac{B_0^2}{4\,\pi}\,V_\mathrm{d}\,b = 2.6\,10^{16} \quad \mathrm{erg\,cm}^{-1}\,\mathrm{s}^{-1}\,.$$

$$\mathrm{SF} = f(\theta)\,\frac{n\,(k_\mathrm{B}\,T)^{3/2}}{m_\mathrm{i}^{1/2}}\,\xi\,b = 9.8\,10^{15} \quad \mathrm{erg\,cm}^{-1}\,\mathrm{s}^{-1}\,.$$

and therefore $\mathrm{SF/SI} \approx 0.4$ in the test model. The disagreement about the relative roles of heat conduction in the test and new models is due to the fact that in the test model, firstly, SI is less since some part of energy is spent on heating and accelerating ions, and secondly the heat conduction SF is larger here since it is proportional to the function $f(\theta)$, equal to 10.7 for $\theta = 6.5$ (in the test) and 1.0 for $\theta = \infty$ (in the new model).

Thus we conclude that both models show good agreement, giving results of the same order of magnitude. The exception

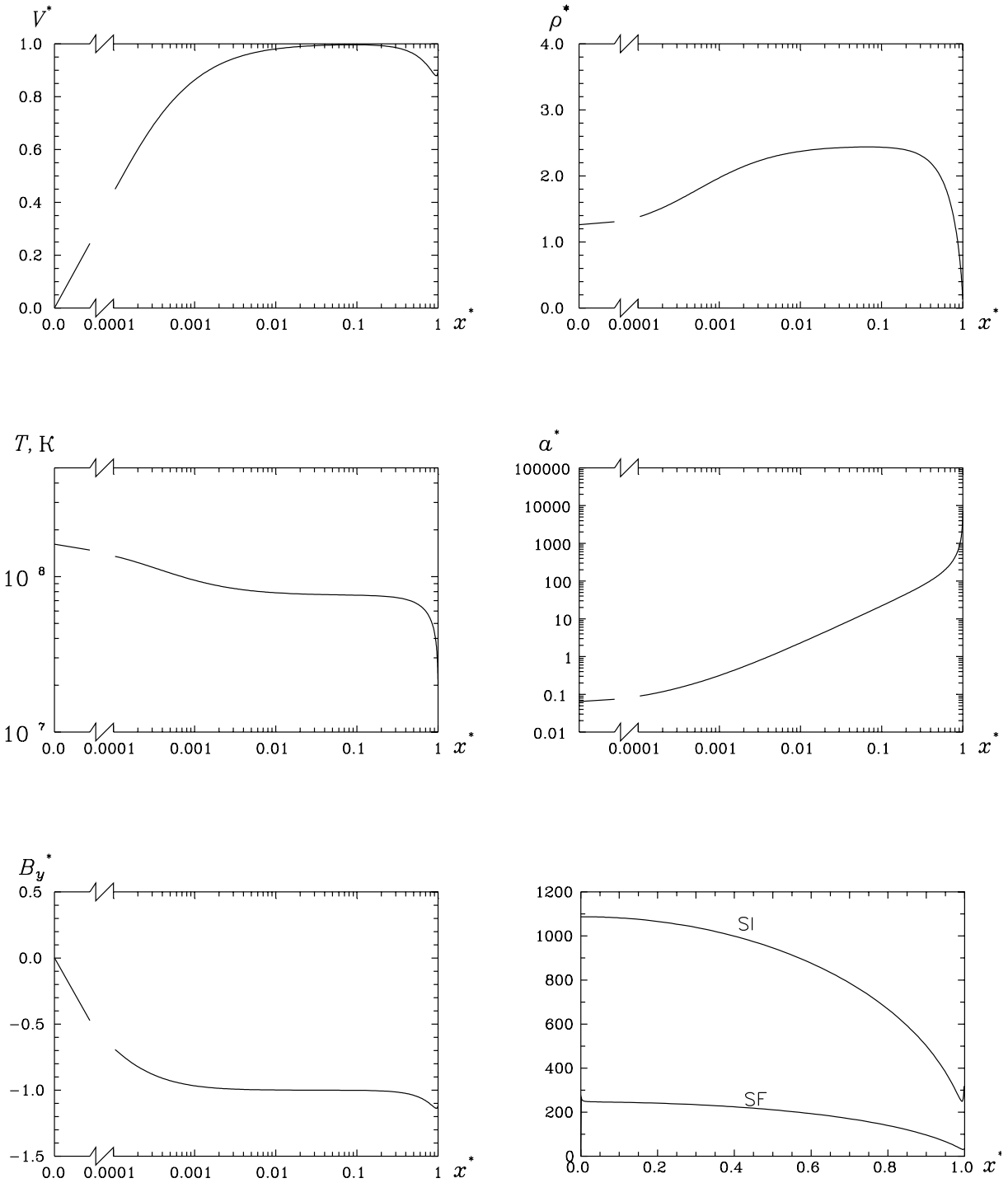

Fig. 8. New model of HTCS computed for external plasma parameters adopted in the test model

constitutes the sheet thickness and hence the region of anomalous resistivity which has increased by three orders of magnitude in the new model comparing with the test and equals $\sim 10^5$ cm. This discrepancy is due to somewhat different sets of the problems.

In conclusion continuing on from the Paper I which presents computations for the low-temperature ($T \sim 10^4$ K) current sheet, where the high-temperature ($T \sim 10^8$ K) sheet was established to be unstable. Taking into consideration the results obtained to date, it can be concluded that two possible causes excite this instability. First, it is an inadequate resistivity, which has been taken in the classical form (it is valid at the temperature of about 10^4 K but invalid at 10^8 K). Second, the role of radiative losses has been taken very high ($\alpha_{\rm r} = 1$), whereas the estimations described above give $\alpha_r \lessapprox 10^{-2}$. Radiation, as is known, may give rise to instability. Allowance for these factors

results in stable solutions, which have been demonstrated in the present paper.

So, a new MHD model of the reconnecting current sheet is proposed that takes into account anomalous resistivity of plasma, radiative cooling, and anomalous heat conduction. It demonstrates the possibility of the existence of high-temperature turbulent-current sheet under the conditions of solar corona and enables us to study its structure (variations of plasma parameters along the sheet width). The model describes two regimes of reconnection: the slow one with O-type magnetic configuration and the fast one with X-type configuration. Energy release power in the sheet at the fast regime is sufficient to account for solar flares and coronal transients.

References

Buneman O., 1958, Phys. Rev. Letters 1, 8

Cox D.P., Tucker W.H., 1969, ApJ 157, 1157

Heyvaerts J., Priest E.R., 1976, Solar Physics 47, 223

de Kluiver H., Perepelkin N. F., Hirose A., 1991, Physics Reports 199, No. 6, 281

Kosugi T., Somov B.V., 1998. In: Watanabe T., Kosugi T., Sterling A.C. (eds.) Observational Plasma Astrophysics: Five Years of Yohkoh and Beyond. Kluwer Academic Publ., Dordrecht, Boston, London, 297

Magara T., Shibata K., 1997, Adv. Space Res. 19, No. 12, 1903

Manheimer W. M., 1977, The physics of fluids 20, No. 2, 265

Manheimer W. M., Klein H. H., 1975, The physics of fluids 18, No. 10, 1299

Masuda S., Kosugi T., Hara H., et al., 1994, Nat 371, 495.

Mewe R., Lemen J., van den Oord G.H.J., 1986, A&AS 63, 511

Neukirch T., Dreher J., Birk G. T., 1997, Adv. Space Res. 19, No. 12, 1861

Oreshina A.V., Somov B.V., 1998, A&A 331, 1078 (Paper I)

Raymond J.C., Cox D.P., Smith B.W., 1976, ApJ 204, 290

Schumaher J., Kleim B., 1997, Adv. Space Res. 19, No. 12, 1797

Shmeleva O. P., Syrovatskii S. I., 1973, Solar Physics 33, 341

Somov B.V., 1992, Physical Processes in Solar Flares, Kluwer Academic Publ., Dordrecht, Holland

Somov B.V., 1994, Fundamentals of Cosmic Electrodynamics, Kluwer Academic Publ., Dordrecht, Boston, London

Syrovatskii S. I., 1971, Soviet Physics - JETP 33, 933

Takakura T., 1990, Solar Physics 127, 95

Takakura T., 1992, Solar Physics 142, 327

Takakura T., Inda M., Makishima K. et al., 1993, PASJ 45, 737

Watanabe T., Kosugi T., Sterling A.C. (eds.), 1998, Observational Plasma Astrophysics: Five Years of Yohkoh and Beyond, Kluwer Academic Publ., Dordrecht, Boston, London